COBEM 2021 26th International Congress of Mechanical Engineering
ABCM Associação Brasileira de Engenharia e Ciências Mecânicas
November 22-26, 2021, Virtual Congress, Brazil

COB-2021-1749
STRUCTURAL ANALYSIS OF A FILAMENT WOUND ROCKET MOTOR CASING UNDER INTERNAL PRESSURE

Erika Kamada Tomita
Artem Andrianov
Aerospace Engineering Course, University of Brasília, Área Especial de Indústria Projeção A, Setor Leste, Gama, Brazil, 72444-240.
erika.kamadat@gmail.com, andrianov@aerospace.unb.br

Abstract. *The paper presents the structural behavior of a filament-wound casing under internal pressure by finite element method (FEM). The numerical model includes a cylindrical casing with hemispherical domes and port openings of the same diameter subjected to internal pressure. The model represents the combustion chamber of a low-thrust hybrid propellant rocket motor. The winding angle is determined by a geodesic trajectory of the fiber and depends on the preselected casing geometry in accordance with Clairaut equation. Thickness variation at flanges of the domes is in conformity with so-called flat solution. The model is used to determine the influence of stacking sequence of the casing's laminate on 1) the hoop strain at the interface of cylinder with hemispherical dome and 2) the value of inverse reverse factor (IRF) at the center of the cylinder. The carbon/epoxy coupons $[0]_5$ are fabricated by filament winding to measure tensile mechanical properties and evaluate the fiber volumetric content by optical technique based on image analysis of micrographs. These data are used to evaluate the minimal rupture thickness of the casing.*

Keywords: *structural analysis, composite rocket case, pressure vessel, filament winding.*

NOMENCLATURE

b – tow width;
E_1 – longitudinal elasticity modulus;
E_{1f} – tensile modulus of the fiber;
E_2 – transverse elasticity modulus;
F_{1t} – measured mean value of the tensile strength of the unidirectional laminate
F_{1f} – tensile strength of the fiber;
F_{1t}^* – theoretical tensile strength of the unidirectional laminate calculated by netting theory ($= F_{1f}V_f$);
F_{2t} – transverse tensile strength;
R_c – radius of the cylindrical casing and hemispherical dome;
r_p – radius of polar opening;
t – test coupon thickness;
t_{do} – thickness in the dome near the opening;
t_d – thickness distribution in the dome (excluding the portion near the opening) as a function of the z-coordinate;
t_h – thickness of hoop layer;
t_{hn} – minimum required thickness of hoop layers given by netting theory;
t_α – thickness of angle ply $\pm\alpha$;
$t_{\alpha n}$ – minimum required thickness of angle ply $\pm\alpha$ given by netting theory;
x_p – x-coordinate of the polar opening
α – winding angle on the cylindrical part;
$\alpha_s(x)$ – winding angle on the hemispherical dome as a function of the x-coordinate;
ρ_f – linear mass density of the fibers.

ACRONYM

CV – Coefficient of Variation
FEM – Finite Element Method
FPF – First Ply Failure
IRF – Inverse Reverse Factor

1. INTRODUCTION

The use of filament winding for manufacturing of composite rocket motors has been known since 60s (Gaubatz, 1965) and continues nowadays (Betti *et al.*, 2007; Crapiz, 1991; Drain *et al.*, 1994; J. Park *et al.*, 2002). The effect from replacing metallic casing by a composite one is associated with a significant reduction in mass for the same ballistic performance of the motor. Thus, for instance, 30% of the motor mass is reduced for the Evolved Sea Sparrow (Tenden and Fossumstuen, 2002). Despite this, composite materials do not always show better structural performance: most of the Northrop Grumman low thrust motors are made from light metal alloys such as aluminum and titanium ("Propulsion products catalog", 2016). The combination of composite material with metallic liner is another solution to combine structural performance with long-term integrity of the casing, but this design is more common for pressure vessels that require high degree of impermeability (Hardy and Malik, 1990).

The current work is a part of preselection process of the filament wound composite casing for a low-thrust hybrid propellant motor of the propulsive decelerator described in reference (Andrianov *et al.*, 2015). At the given phase, it is considered that the thrust of the decelerator is small in relation to internal pressure of 3 MPa. The casing consists of a cylinder with hemispherical domes and port openings of the same diameter (Figure 1).

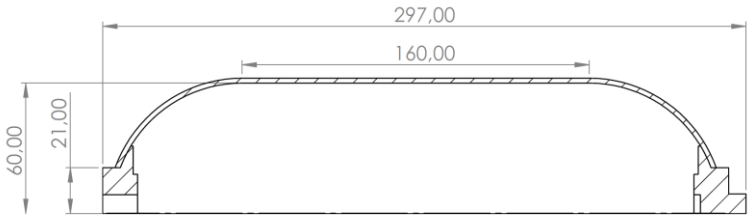

Figure 1. Dimensions of the casing, in mm.

The closed opening of the casing indicates that the model is intended for a hydrostatic test. There is no axial restrain for the casing since the motor is fixed only at the end face of one of the flanges. Massive flanges are chosen to increase rigidity in the region of the polar openings with the aim to create severe loading conditions for the casing. The casing is manufactured by filament winding of the hoop and helical plies, whose order of application depends on stacking sequence.

The main objective of this work is to determine the influence of stacking sequence of the casing's laminate on 1) the hoop strain at the interface of cylinder with hemispherical dome and 2) the first ply failure (FPF) at the center of the cylinder.

One of the criteria for optimal design of a pressure vessel requires compatibility in the dome-cylinder transition, which is reached by a proper combination of the thicknesses of helical and hoop layers. If the above condition is not followed, disagreement between hoop strains may significantly decreases the pressure of rupture for the vessel (Özaslan *et al.*, 2018; J. Park *et al.*, 2002; J. S. Park *et al.*, 2002). Some authors employ dome reinforcements to avoid this effect (Özaslan *et al.*, 2018; J. Park *et al.*, 2002). At initial phase of development, the compatibility can be obtained by an iterative analytical method (Koussios, 2011). However, as the iteration process is labor-intensive and time-consuming, observation of the compatibility in the given work is done through the analysis of a numerical model of the casing by finite element method. The secondary objective of the work is to evaluate the minimal thickness of the casing at which the rupture may occur for the given loading conditions.

2. MATERIAL AND METHODS

2.1 Evaluation of casing rupture thickness

The minimal required thicknesses t_{hn} and $t_{\alpha n}$ of the hoop and helical plies $\pm\,\alpha$, respectively, are determined by the netting theory (Tew, 1995)

$$t_{\alpha n} = \frac{pR_c}{2F_{1t}^{*}\cos\alpha}$$
$$t_{hn} = \frac{pR_c}{2F_{1t}^{*}}(2-\tan^2\alpha) \qquad (1)$$

In Equation (1), laminate unidirectional strength F_{1t}^{*} is reduced by 25% due to cracks in resin, stress concentrating effects, fiber weaving, etc in accordance with recommendations given in (Tew, 1995)

$$F_{1t}^{*} = 0.75F_{1t} \quad (2)$$

Here, F_{1t} is measured mean value of the tensile strength of the manufactured unidirectional laminate.

2.2 Material characterization

Carbon fiber Teijin Carbon HTS45 E23 12K based on polyacrylonitrile (Table 1) and epoxy composition Huntsman LY1564/XB3473 are used to fabricate the unidirectional laminate. The longitudinal tensile properties are measured in accordance with ASTM 3039/D3039M-00, with use of testing machine Instron 8801 and strain gauge Instron 2620-601 (maximum displacement of 12.5 mm), at displacement rate of 2 mm/min. The test coupons of the unidirectional laminate $[0_5]$ are wound in five successive layers onto a rectangular aluminum mandrel with dimensions of 300x160x10 mm, then cut to dimensions 240x15x1 mm. Thickness is obtained by adjusting the distance between two flat plates of the mechanical press. Curing process consists of 30 minutes at 130ºC and 12 hours at 160ºC in an electric oven. The thickness is measured by Mutitoyo digital caliper with resolution of 0.01 mm. Thickness of one ply is given by the ratio between laminate thickness and number of the wound plies.

Table 1. Carbon fiber tow properties (as declared by local supplier).

Parameter	Minimal	Nominal	Maximal
$\boldsymbol{\rho_f}$, tex	720	800	880
$\boldsymbol{\rho}$, g/cm^3	1.77	1.80	1.83
$\boldsymbol{F_{1f}}$, MPa	4050	4500	4950
$\boldsymbol{E_{1f}}$, GPa	228	240	252

The fiber volumetric content is determined by an optical technique based on the analysis of micrographs of the coupons' cross-sections. Volume ratio is given by the total area of the fiber cross-sections over the image area. ImageJ free software is used to determine the area of the fiber cross-sections using an 8-bit micrograph at 400x magnification (Figure 2).

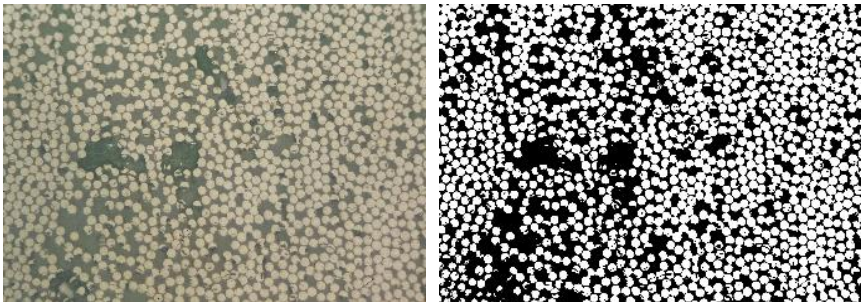

(a) (b)

Figure 2. Example of a 400x micrograph of the laminate $[0_5]$ (a) before and (b) after treatment in ImageJ. White areas represent fibers, whose volume ratio corresponds to 52.7% in the image (b).

2.3 Numerical model

The numerical model is done in Ansys Composite Pre-Post following the dimensions given in Figure 1. The model represents a combination of the casing meshed predominantly with shell 181 element and flanges meshed with solid 186 element. Mechanical properties of the material used for the composite casing are given in Table 2. The material of the flanges is aluminum alloy (modulus of elasticity is 71 GPa and the Poisson's ratio is 0.33).

Table 2. Mechanical properties of carbon fiber/epoxy resin composite ("ANSYS Engineering data source", [s.d.]).

E_1 GPa	E_2, E_3 GPa	G_{12}, G_{13} GPa	G_{23} GPa	ν_{12}, ν_{13}	ν_{23}
123.34	7.78	5	3.08	0.27	0.42
F_{1t} MPa	F_{2t}, F_{3t} MPa	F_{12}, F_{13} MPa		F_{23} MPa	
1632	34	80		55	

Boundary conditions consist of internal pressure of 3 MPa and one of the flanges fixed by its external end face.

The data for the hoop strain of the model are obtained for the last helical layer of the casing. The failure analysis is based on first ply failure (FPF) associated with the maximum stress criteria. Inverse reserve factor (IRF) is used as an indicator of failure at the center of the cylinder.

2.3.1 Winding angle

Winding angle at each point of the dome is given by geodesic path (Koussios, 2011) in accordance with the formula

$$\alpha_s(x) = \arcsin \sqrt{\frac{R_c^2 - x_p^2}{R_c^2 - x^2}} \tag{3}$$

Filament winding presupposes a lamination sequence ($\pm \alpha$, 90º) (Krikanov, 2000). Helical layers compose the domes and the cylinder, while the hoop layer reinforces the cylinder only. Winding angle at the cylindrical region, α, must satisfy Clairaut equation

$$\alpha = \arcsin \frac{r_p}{R_c} \tag{4}$$

2.3.2 Stackups

According to the formula above, it is intended to analyze the following stacking sequences with enough number of plies to withstand applied internal pressure of 3 MPa: [90/$\pm\alpha_4$], [$\pm\alpha$ /90/$\pm\alpha_3$], [$\pm\alpha_2$/90/$\mp\alpha_2$], [$\pm\alpha_3$/90/$\pm\alpha$] e [$\pm\alpha_4$/90].

2.3.3 Dome thickness distribution

Thickness distribution in the dome is given by so-called flat solution, which can satisfactorily approximate real thickness distribution (Peters, 2011). Thickness in adjacent region to polar opening is constant and defined by

$$t_{do} = \frac{R_c t_c \cos \alpha_s}{\sqrt{b \cos(\alpha_s + \frac{b}{R_c}) \left[2r_p + b \cos\left(\alpha_s + \frac{b}{R_c}\right)\right]}} \tag{5}$$

For the rest of the dome, thickness is a function of the x-coordinate.

$$t_d(x) = \frac{R_c r_p \cos \alpha_s}{\sqrt{R_c^2 - r_p^2 - x^2}} \tag{6}$$

2.4 Validation of the numerical model

Verification of the numerical model is fulfilled by comparing the hoop strain calculated by classical lamination theory (CLT) and FEM. The CLT model is presented by a laminate under biaxial tensile loading, where the principal stresses are defined by theory of thin shells under internal pressure (Daniel and Ishai, 2006). The hoop strains in the CLT model are calculated with use of Octave software in accordance with analytical methodology described in (Daniel and Ishai, 2006). Only longitudinal (E_1, F_{1t}), transversal (E_2, F_{2t}) and in-plane (ν_{12} e G_{12}) properties are considered for the CLT model (Table 2). Since the application of CLT model is limited to the regions far from ends of the cylinder and to symmetric laminates, the hoop strains are compared only at the center of the cylinder for the symmetric laminate [$\pm\alpha_2$/90/$\mp\alpha_2$].

3. RESULTS AND DISCUSSION

3.1 Material characterization

As for the evaluation of tensile longitudinal properties (Table 3), there is a high coefficient of variation. Significant pores size (Figure 3) may have influenced the discrepancy between measurements. Despite the pores has low effect on the longitudinal tensile strength, they reduce the fiber volume ratio. The evaluated mean value for the fiber volumetric ratio is 49.3% (coefficient of variation CV = 8.8%).

Table 3. Longitudinal properties of $[0]_5$ laminate.

t	***F*$_{1t}$**	***CV***	***E*$_1$**	***CV***
mm	MPa	%	GPa	%
1.0	1249	16.9	149.5	26.0

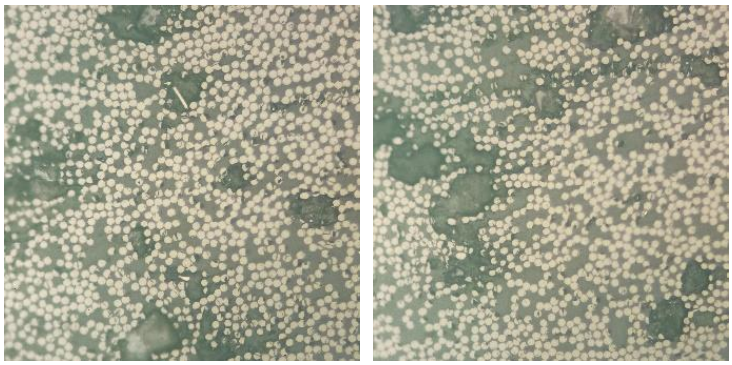

Figure 3. Pores in micrographs at 400x magnification.

3.2 Evaluation of casing rupture thickness

For an internal pressure up to 3 MPa and a safety factor of 1.5, the minimum thickness required for the $\pm \alpha$ and hoop plies is 0.15 and 0.27 mm, respectively. These values are of the same order as the ply thickness measured through the coupons $[0]_5$, which is in the range 0.24 – 0.25 mm.

3.3 Winding parameters

Winding angle $\pm \alpha$ is obtained by Equation 4 and corresponds to 20.5º. Winding angle and thickness distribution at each point of the dome are given in Figure 4 and 5, respectively.

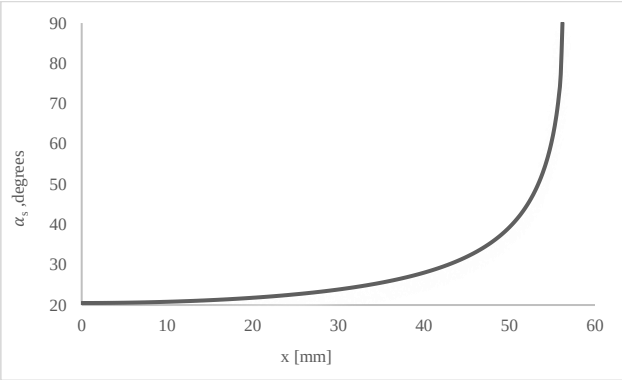

Figure 4. Winding angle α_s as a function of x-coordinate at the dome; x-axis corresponds to the axis of symmetry, where origin corresponds to the dome-cylinder transition.

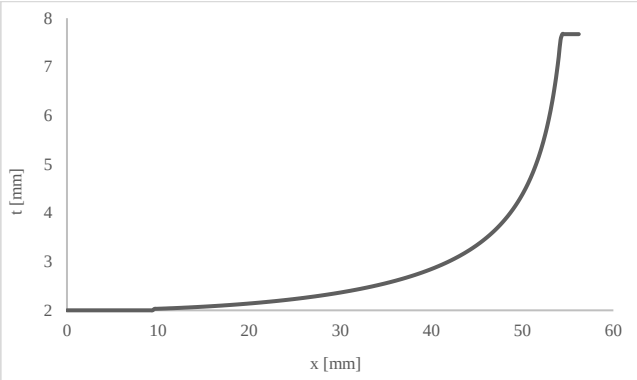

Figure 5. Thickness distribution t as a function of x-coordinate at the dome, for a layer thickness of 0.25 mm; x-axis corresponds to the axis of symmetry, where origin corresponds to the dome-cylinder transition.

3.4 Elastic behavior of the casing

The difference of the hoop strains at the center of the cylinder predicted by FEM and CLT is 0.348% at IRF 0.73 that shows a good agreement of the numerical model with CLT. Thus, numerical model is validated and can be used for structural analysis.

As Figure 6 shows, there is a disagreement in a hoop strain at the dome-cylinder transition (Figure 6). As mentioned above, the effect can be avoided ensuring compatibility at the region by the variation of thickness of hoop and angle-ply layers (Koussios, 2011). However, it is not always possible to carry out the iterative process, since in filament winding technology the layer thickness depends on the roving density. In the present work, the minimal thickness of the ply is 0.25 mm. Figure 7 shows only the obtained combinations of thicknesses that provide compatibility condition at the dome-cylinder transition.

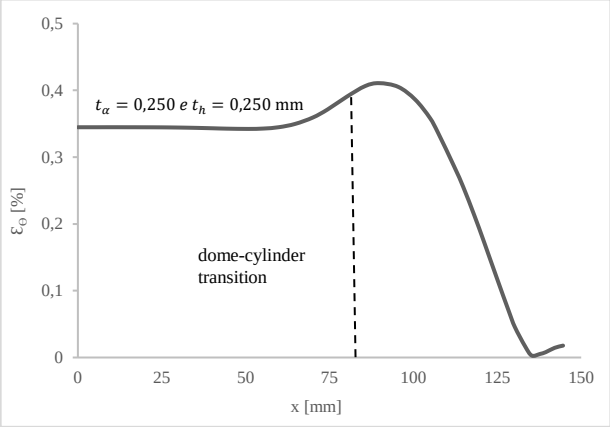

Figure 6. Hoop strain along the axis of symmetry for the last helical layer of the stacking sequence [±20.5$_4$/90]. Origin corresponds to the middle of the casing.

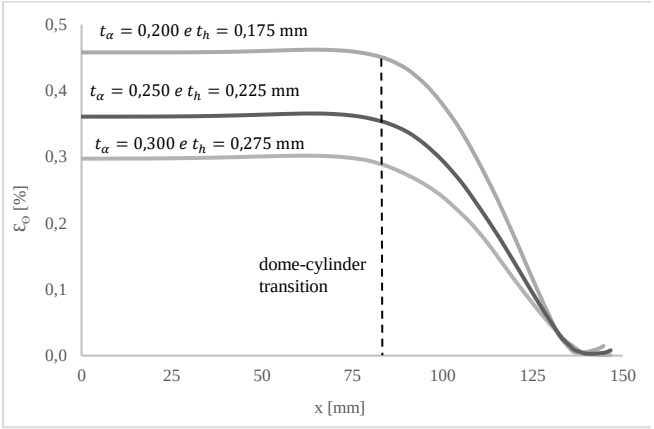

Figure 7. Hoop strain along the axis of symmetry for the last helical layer of the stacking sequence [±20.5$_3$/90/∓20.5$_3$]. Different thickness of layer is considered. Origin corresponds to the middle of the casing.

3.5 FPF Analysis

The values of IRF are very similar for various stacking sequences (Table 4). The failure mode is tensile transverse and the most critical layer corresponds to the last helical layer (Figure 8). The layer strength in this direction is a matrix dominated property (Mehdikhani *et al.*, 2018). For the laminate [$\pm\alpha_2$/90/$\mp\alpha_2$], the maximum IRF of 0.72 in the central region of the cylinder is slightly lower than in the other sequences. This can be caused by the symmetrical nature of this laminate, that is, loads applied to the plane do not cause curvature effects. Furthermore, because the laminate is balanced, there are no in-plane shear strains. However, as the IRF variation is very small, any stacking sequence can be used for the filament winding of the casing. Thus, the lamination sequence for the experimental casing is chosen as required by the technology: the sequence [±20.5$_4$/90] provides continuous winding with only one transition from angle ply to hoop layer (Figure 9).

Table 4. Results of evaluation from numerical analysis.

	Dome-cylinder transition		**Cylinder central region**	
	ε_θ [%]	**IRF**	**ε_θ [%]**	**IRF**
[90/±α_4]	0.428	0.96	0.345	0.73
[±α /90/±α_3]	0.425	0.95	0.345	0.73
[±α_2/90/∓α_2]	0.421	0.93	0.345	0.72
[±α_3/90/±α]	0.420	0.94	0.345	0.73
[±α_4/90]	0.419	0.93	0.345	0.73

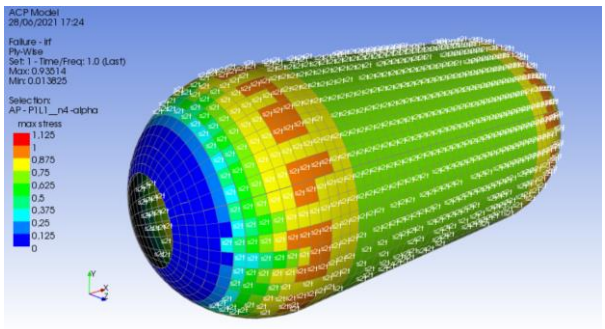

Figure 8. FPF and IRF evaluation of the last helicoidal ply for stacking sequence [±20.5$_4$/90].

Figure 9. Filament wound carbon/epoxy casing with stacking sequence [±20.5$_4$/90] for hydrostatic test.

4. CONCLUSION

Numerical model is obtained to evaluate the structural behavior of the composite casing under internal pressure of 3 MPa for the given geometry of the propulsive decelerator. The validation of the model is done by CLT for the symmetrical and balanced laminate. The error for the evaluation of hoop strain at the center of the cylinder by CLT and FEM is less than 0.35%.

The validated numerical model shows that the stacking sequence does not have a significant influence on structural performance of the casing, however the configuration $[\pm\alpha_4/90]$ provides the least values for the hoop strain ε_Θ=0.419% and IRF=0.93 in the cylinder-dome transition region. Since the tensile transverse failure is predicted, casing leakage is expected to occur at the dome-cylinder transition. At the same time the burst rupture of the casing should not occur, as the minimum rupture thickness evaluated by netting theory is of the same order as the thickness of the ply manufactured by filament winding. The results of the study have permitted to choose the stacking sequence for the experimental casing, which will be subjected to hydrostatic testing.

5. ACKNOWLEDGEMENTS

The authors acknowledge the Foundation of Research Projects in the Federal District (FAP DF) and the University of Brasilia Foundation (FUB) for the financial support of the project and Post-Graduation Department of the UnB (DPG-ProIC) for the technical support.

6. REFERENCES

Andrianov, A., Shynkarenko, O., Bertoldi, A. E. M., Barcelos, M. N. D., e Veras, C. A. G. (2015) Concept and design of the hybrid test-motor for the development of a propulsive decelerator of SARA reentry capsule. *51st AIAA/SAE/ASEE Joint Propulsion Conference*.

ANSYS Engineering data source. ([s.d.]).

Betti, F., Perugini, P., Mataloni, A., Tessitore, N., Leone, A., Di Cosmo, A., Vari, E., Bonnet, M., e Di Vita, G. (2007) Design and development of VEGA solid rocket motors composite cases. *43rd AIAA/ASME/SAE/ASEE Joint Propulsion Conference*. Cincinnati, OH.

Crapiz, D. (1991) Procédé de fabrication d'une chambre de combustion de propulseur a propergol solide.

Daniel, I. M., e Ishai, O. (2006) *Engineering mechanics of composite materials*. (Second Edi.). Oxford University Press, New York - Oxford.

Drain, K. F., Nativiti, L. A., e Thompson, R. T. (1994) Solid fuel rocket motor assembly, and method of making the same.

Gaubatz, A. W. (1965) Filament winding of rocket cases. United States. doi:10.1145/178951.178972

Hardy, S. J., e Malik, N. H. (1990) Optimum Design of Composite-Reinforced Pressure Vessels. *Applied Stress Analysis*. Springer.

Koussios, S. (2011) Integral design for filament winding—materials, winding patterns, and roving dimensions for optimal pressure vessels. S. T. Peters (Ed), *Composite Filament Winding*. ASM International, Ohio.

Krikanov, A. A. (2000) Composite pressure vessels with higher stiffness. *Composite Structures, 48*.

Mehdikhani, M., Gorbatikh, L., Verpoest, I., e Lomov, S. V. (2018) Voids in fiber-reinforced polymer composites: A review on their formation, characteristics, and effects on mechanical performance. *Journal of Composite Materials*.

Özaslan, E., Acar, B., e Yetgin, A. (2018) Design and validation of a filament wound composite rocket motor case. *PVP2018 Proceedings of the ASME 2018 - Pressure Vessels and Piping Conference*. Prague, Czech Republic.

Park, J., Kim, C., Kang, H., Hong, C., e Kim, C. (2002) Structural Analysis and Strain Monitoring of the Filament Wound Motor Case. *Journal of Composite Materials*, *36*(20), 2373–2388.

Park, J. S., Hong, C. S., Kim, C. G., e Kim, C. U. (2002) Analysis of filament wound composite structures considering the change of winding angles through the thickness direction. *Composite Structures*, *55*(1), 63–71.

Peters, S. T., 2011. *Composite Filament Winding*. ASM International.

Propulsion products catalog. ([s.d.]). Northrop Grumman.

Tenden, S., e Fossumstuen, K. (2002) IM Improvement of rocket motor by composite motor case. *RTO AVT Specialists Meeting on "Advances in Rocket Performance Life and Disposal"* (p. 22-(1-14)). Aalborg, Denmark. Obtido de https://www.sto.nato.int/publications/STO Meeting Proceedings/RTO-MP-091/MP-091-22.pdf

Tew, B. W. (1995) Preliminary design of tubular composite structures using netting theory and composite degradation factors. *Transactions of the ASME, 117*.

7. RESPONSIBILITY NOTICE

The authors are the only responsible for the printed material included in this paper.